Nanoscale manipulation of Ge nanowires by ion irradiation

Lucia Romano,[1,a)] Nicholas G. Rudawski,[2,b)] Monta R. Holzworth,[2] Kevin S. Jones,[2] S. G. Choi,[3,c)] and S. T. Picraux[3]

[1]*Department of Physics and Astronomy, University of Catania and MATIS CNR-INFM, 64 Via S. Sofia, I-95123 Catania, Italy*

[2]*Department of Materials Science and Engineering, University of Florida, Gainesville, Florida 32611, USA*

[3]*Center for Integrated Nanotechnologies, Los Alamos National Laboratory, Los Alamos, New Mexico 87545, USA*

(Received 28 September 2009; accepted 2 November 2009; published online 10 December 2009)

Nanowires have generated considerable interest as nanoscale interconnects and as active components of both electronic and electromechanical devices. However, in many cases, manipulation and modification of nanowires are required to fully realize their potential. It is essential, for instance, to control the orientation and positioning of nanowires in some specific applications. This work demonstrates a simple method to reversibly control the shape and the orientation of Ge nanowires using ion beams. Crystalline nanowires were amorphized by 30 keV Ga^+ implantation. Subsequently, viscous flow and plastic deformation occurred causing the nanowires to bend toward the beam direction. The bending was reversed multiple times by ion implanting the opposite side of the nanowires, resulting in straightening and subsequent bending into that opposite direction. This effect demonstrates the detailed manipulation of nanoscale structures is possible through the use of ion irradiation. © *2009 American Institute of Physics*. [doi:10.1063/1.3267154]

I. INTRODUCTION

Crystalline Ge nanowires (NWs) can be grown by vapor-liquid-solid (VLS) epitaxy with Au catalyst nanoparticles resulting in pillars with nanometer-scale diameters and high aspect ratios.[1] The NWs exhibit exceptional mechanical and electrical properties that are attractive for a variety of applications (field-effect transistors, light emitting diodes, spintronic devices, photovoltaic cells, and chemical sensors).[2–7] The key to the future success of one-dimensional nanotechnologies is assembly, or the art of putting nanostructures where one desires, with the desired connectivity, and nowhere else. Nanostructure assembly is challenging because the pertinent length scales prohibit any direct tinkering. Thus, it is highly desirable to be able to precisely manipulate the orientation of either individual NWs or an entire surface covered with NWs. This work introduces and investigates the application of ion-beam processing as a simple method to control and manipulate the orientation and the shape of a NW after growth.

The damage from ion irradiation is usually an undesirable phenomenon, unless used for preamorphizing a material, such as Si, prior to doping.[8] One might expect that irradiation should have the same effects on nanosystems as bulk solids. However, recent experiments on electron and ion irradiations of various nanomaterials demonstrate the ability to tailor the structure and properties of nanosystems with high precision.[9] No demonstrated effect of ion irradiation on NWs has yet been reported.

When an energetic ion penetrates a solid, it loses energy mainly via two independent processes, with the relative magnitude of each process related to the ion velocity: (i) nuclear energy loss (S_n), which dominates at low energy and results from a direct transfer of kinetic energy to the target nuclei (elastic collisions), and (ii) electronic energy loss (S_e), which prevails at high energy and results from electronic excitation and/or ionization of the target atoms (inelastic collisions).[10] In some cases, energetic ion bombardment of amorphous thin films results in unsaturable plastic flow in the form of anisotropic deformation with negligible density change (ion hammering effect). In this case, the ion beam induces compressive (tensile) deformation parallel (perpendicular) to the beam direction for sufficiently high S_e (≥ 1 keV/nm) and sufficiently low target temperatures.[11] Another effect is the densification of the irradiated material which has been reported in SiO_2 and appears to be the result of both electronic and nuclear energy losses. The densification process has been shown to saturate when an energy density $\sim 10^{20}$ keV/cm^3 is deposited into atomic collisions.[12] Here, we show that ion irradiation (30 keV Ga^+ implantation in Ge) may be used to precisely alter nanoscale structures with the results explainable by the predictions of ion hammering where the material has a negative thermal expansion coefficient or alternatively with a 5% densification of the irradiated material.

II. EXPERIMENTAL

NWs used in this study were grown epitaxially via the VLS mechanism in a high-vacuum cold-wall chemical vapor deposition (CVD) system on (111) Si.[13] To facilitate the transmission electron microscopy (TEM) examination, the NWs were grown on (111) Si pillars ~ 40 μm tall and ~ 2 μm in diameter. The pillars were prepared by deep reactive ion etching of a lithographically patterned (111) Si

[a)]Author to whom correspondence should be addressed. Electronic mail: lucia.romano@ct.infn.it.

[b)]Also at University of California, Santa Barbara, Santa Barbara, California 93106, USA.

[c)]Also at National Renewable Energy Laboratory, Golden, Colorado 80401, USA.

 © 2009 American Institute of Physics

Downloaded 17 Mar 2011 to 128.227.165.227. Redistribution subject to AIP license or copyright; see http://jap.aip.org/about/rights_and_permissions

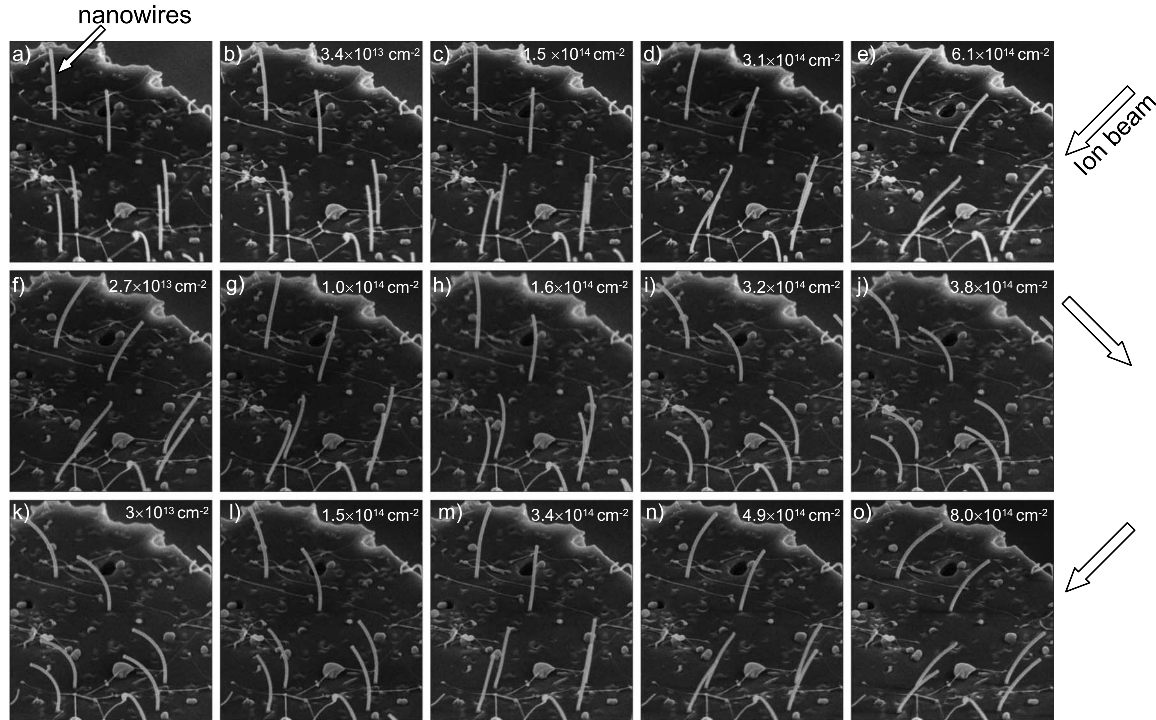

FIG. 1. SEM images of three ion irradiation sequences (a video is available as multimedia file) showing reversible bending of Ge NWs epitaxially grown on (111) Si during Ga^+ irradiation at 30 keV incident at 45° with respect to the vertical of the NWs. Ion-beam incident from the right with Q=: (a) 0 (as-grown, nonirradiated), (b) 3.4×10^{13}, (c) 1.5×10^{14}, (d) 3.1×10^{14}, and (e) 6.1×10^{14} cm^{-2}. Ion beam subsequently incident from the left on the resulting NWs with additional Q=: (f) 2.7×10^{13}, (g) 1.0×10^{14}, (h) 1.6×10^{14}, (i) 3.2×10^{14}, and (j) 3.8×10^{14} cm^{-2}. Ion beam subsequently incident from the right on the resulting NWs with Q=: (k) 3.0×10^{13}, (l) 1.5×10^{14}, (m) 3.4×10^{14}, (n) 4.9×10^{14}, and (o) 8.0×10^{14} cm^{-2}.

substrate. After forming the pillars, 5×8 mm^2 coupons of the Si substrate containing a 6×6 array of pillars were cleaved. Then the coupons were cleaned with acetone followed by methanol rinse in order to remove the residual photoresist. Even though a small number of craters were present on the top surface of the pillars, enough flat Si (111) surface region remained, which enabled growth of epitaxial Ge NWs on the top of the pillars. Prior to loading into the CVD chamber, the native oxide on the Si pillars was removed by a dilute hydrofluoric (HF) acid (2 vol % in deionized water) dip and acidified Au nanoparticles with a nominal diameter of 50 nm were dispersed on the coupons. The coupons were further outgassed at 200 °C inside the CVD chamber under vacuum (mid-10^{-8} Torr range) for 5 h and preannealed at 450 °C for 10 min immediately before growth. The growth of Ge NWs proceeded via a "two-step" growth where the growth was initialized at 425 °C and subsequently continued at 375 °C. This procedure was shown to increase the proportion of vertically aligned Ge NWs while ensuring minimum tapering. GeH_4 (30% in H_2) was used as the process gas with a partial pressure of 900 mTorr during the growth. The growth duration was 10 min. The Ge NWs grew along the four ⟨111⟩ directions with only the ones grown normal to the surface (i.e., [111] direction) used in this study.

A FEI Strata DB 235 scanning electron microscope/focused ion-beam (FIB) system was used to perform *in situ* ion-beam irradiation. Electron and ion beams were oriented with an angle of 52° between them. The stage was tilted in order to vary the ion-beam direction with respect to the NWs. The NWs were irradiated at a stage tilt such that the ion beam was incident at 45° relative to the vertical of the NWs. All irradiations were performed using a 30 keV Ga^+ beam with a square scanning pattern of 38×38 μm^2, a current of 10 pA (corresponding to an ion of flux 3 $\times10^{12}$ ions cm^{-2} s^{-1}), a dwell time of 0.1 μs, and a beam spot size of 30 nm. Thus, the dose received depended on the time of exposure and ion-beam incidence angle. After each irradiation step, the stage was tilted to 52° off normal to the electron beam and rotated 90°, in order to take SEM images of the NWs perpendicular to the beam direction.

TEM was used to characterize the structure of the NWs in the as-grown condition and after ion irradiation. The samples were imaged on a Jeol 2010F transmission electron microscope using on-axis, multibeam imaging conditions. The pillar was attached to an *in situ* micromanipulator by selective ion-beam Pt deposition and lifted out from the Si coupon, taking care to avoid any ion-beam irradiation on the top of the pillar in order to protect the NWs. The free pillar was then attached to a special Cu grid and loaded into the microscope for imaging.

III. RESULTS AND DISCUSSION

Ge NWs were Ga^+ irradiated at 30 keV (S_e ~0.1 keV/nm) with the beam incident at 45° relative to the elongated direction of the NWs. Figure 1 (a video related to this figure is available as multimedia file) presents a series of scanning electron microscopy (SEM) images of the gradual and, ultimately, spectacular bending of the Ge NWs under

Downloaded 17 Mar 2011 to 128.227.165.227. Redistribution subject to AIP license or copyright; see http://jap.aip.org/about/rights_and_permissions

Ga^+ irradiation at different doses (Q). With the Ga^+ beam incident from the right with $Q=3.4\times10^{13}$ cm^{-2}, the NWs initially start to bend slightly toward the left, as shown in Fig. 1(b), therefore implying that the irradiated side is subjected to compressive stress coincident with the elongated NW direction. After an ion dose of $Q=1.5\times10^{14}$ cm^{-2}, the NWs are almost vertical [see Figs. 1(c) and 1(d)] and tending to bend toward the right (beam direction) which implies the irradiated side is now experiencing a tensile stress. The gradual bending toward the beam direction is clearly evident in Figs. 1(d) and 1(e) after $Q=3.1\times10^{14}$ and 6.1×10^{14} cm^{-2}, respectively. The deformation is stable after stoppage of irradiation. After irradiation to $Q=6\times10^{14}$ cm^{-2} from the right, the beam direction was reversed in order to impinge from the left, as indicated by the arrows in Figs. 1(f)–1(j) which correspond to additional doses of $Q=2.7\times10^{13}-3.8\times10^{14}$ cm^{-2}. A complete reversal of the bending is observed with the NWs bending toward the beam direction, again implying that the irradiated side of the NW is experiencing a tensile stress. Once again reorienting the beam to impinge from the right, the NWs were once again observed to bend toward the beam, as shown in Figs. 1(k)–1(o), corresponding to $Q=3.0\times10^{13}-8.0\times10^{14}$ cm^{-2} and again implying that the irradiated side is experiencing tensile stress. A decrease in NW diameter due to sputtering was observed for doses greater than 3×10^{15} cm^{-2} for the Ga^+ beam perpendicular to the NWs, while for the NWs aligned parallel to the beam direction much higher doses were possible without observable loss of Ge. The irradiated dose was lower than that necessary to create a swelled porous structure.[14] Furthermore, we did not observe any porous structure or macroscopic voids on the Ge NW surfaces after irradiation. Thus, the NW shape can be manipulated numerous times by ion irradiation without sputtering limitations and is estimated to survive at least twice the 3 cycles demonstrated here.

Related ion-beam-induced bending effects have been reported for carbon nanotubes having diameters from a few to several hundred nanometers[15,16] and for the Si_3N_4 membranes (i.e., the irradiated side of the structure appeared to be experiencing tensile stresses).[17] Park *et al.*[15] discussed mechanisms involving dipole-to-field interaction but have concluded that the electric fields generated are too low to cause the bending. Tripathi *et al.*[16] proposed a model to explain the bending phenomenon which is based on an irradiation-induced temperature rise and temperature gradient produced along the length and breadth of the structure. However, this model assumes that the material has a negative thermal expansion coefficient, and bulk Ge has been shown to have a positive coefficient over a broad temperature range (albeit while not being subjected to ion irradiation).[18]

The amorphization process of the Ge NWs is presented in Fig. 2. Figures 2(a)–2(c) show the SEM and TEM images of an as-grown NW indicating a single crystal of Ge with a diameter of 50 nm and the $\langle 111\rangle$ axis oriented along the wire direction. Partial amorphization of the NW was observed after an implanted dose of $Q=3.5\times10^{13}$ cm^{-2}, which coincided with the initial bending of the NW away from the beam direction, as shown in Fig. 1(d). Ge is known to exhibit

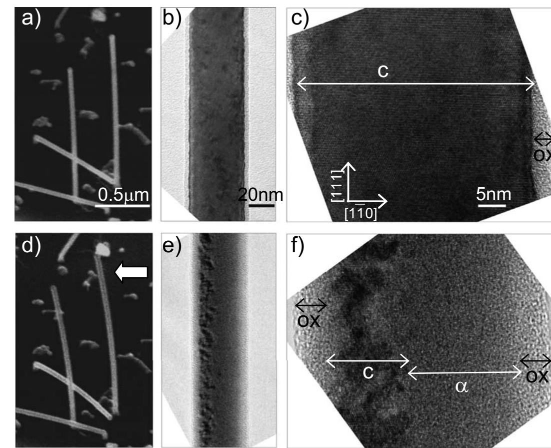

FIG. 2. Effect of low dose implantation on the side of the NW. Before implantation: (a) SEM image, (b) low magnification TEM micrograph, and (c) high-resolution TEM micrograph. After 30 keV Ga^+ implantation at 45° with respect to the NW axis at a dose of $Q=3.5\times10^{13}$ cm^{-2}: (d) SEM image, (e) low magnification TEM micrograph, and (f) high-resolution TEM micrograph. Crystalline (c), amorphous (α) and oxidized (ox) portions of the NWs are schematically indicated; the ion-beam direction is from the right.

an ~10% expansion upon amorphization[14] and thus expansion of the amorphized side is constrained by the crystalline side (compressively stressed) causing the NW initially to bend away from the beam. SEM and TEM imagings indicated that bending appears more accentuated near the top of the NW, presumably due to the base being additionally constrained by the substrate. Low- and high-resolution TEM images, shown in Figs. 2(e) and 2(f), indicated uniform implantation along the one side of the NW and amorphization of approximately two-thirds of the structure, thus indicating that amorphization proceeds from the beam-exposed side of the implanted NW. It should be noted that NWs are three-dimensional structures that can be approximated as a cylinder. Therefore, the surface exposed to the ion beam is curved and the beam incidence becomes more grazing moving from the center of the NW toward the side. Consequently, the implanted ions have a cylindrical distribution. The distribution of 30 keV Ga^+ ions implanted at 0° (45°) tilt into a planar Ge substrate covered with 5 nm GeO_2 (as observed in Fig. 3) has a projected range and a longitudinal range straggling of ~18 (14) and 9 (8) nm, respectively, as calculated by SRIM simulations.[19] Thus, simulations predict an amorphous layer ~25 nm thick. However, since TEM analysis is averaged over the whole NW thickness, the observed depth is larger than the SRIM value. Ultimately, the NWs were completely amorphized after $Q\sim1.0\times10^{14}$ cm^{-2} (not shown) in agreement with the reported bulk Ge amorphization threshold dose by Si^+ implantation at 40 keV at room temperature.[20]

Once completely amorphized, the NWs exhibit gradual bending toward the ion beam direction (implying that the irradiated side is now experiencing tensile stress). Moreover, this deformation was reversible as NWs bent toward the right were subjected to additional irradiation from the left and then bent toward the left. Several SEM images at different tilts and rotation angles were collected in order to identify the

Downloaded 17 Mar 2011 to 128.227.165.227. Redistribution subject to AIP license or copyright; see http://jap.aip.org/about/rights_and_permissions

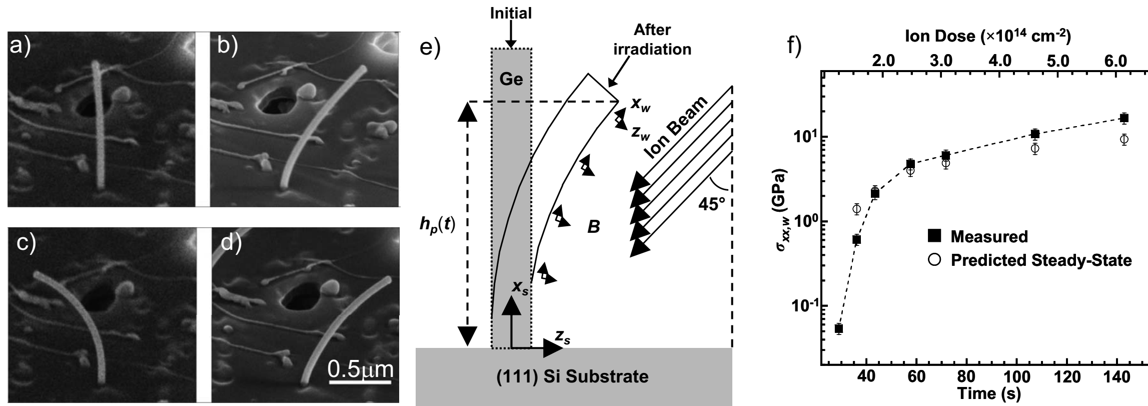

FIG. 3. SEM images showing the reversibility of bending at three different extremes for a single Ge NW during Ga^+ irradiation at 30 keV: (a) an as-grown Ge NW, (b) after irradiation from the right with a dose of $Q=6.1\times10^{14}$ cm^{-2}, (c) after irradiation from the left with $Q=3.8\times10^{14}$ cm^{-2}, and (d) after irradiation from the right with $Q=8.0\times10^{14}$ cm^{-2}. Each value of additional dose Q is given with respect to a specific beam direction (left or right). (e) Schematic discretization of a bending Ge NW shown in (b) depicting the coordinate systems used for the measurement of internal stresses and mechanical work performed during ion irradiation. (f) Plot of the measured in-plane tensile stress, $\sigma_{xx,w}$, (open circles) generated in the NW as determined from the curvature along the bottom portion of the NW shown in (b) as a function of ion dose and irradiation time during the initial irradiation step using Eq. (3). The magnitudes of the predicted (compressive) steady-state values of $\sigma_{xx,w}$ from ion hammering (solid squares) that would be generated in the NW (corresponding to observed irradiation angles at specific times and doses) as predicted by Eq. (1) are provided for reference.

three-dimensional movement of the NWs during bending (not presented). It was revealed that almost all of the bending occurs directly toward the ion beam. However, there are small differences in the NW length (between 10% and 20%) observed between each extreme due to a small amount of torsion that can be caused by a slight misalignment of the FIB stage after each irradiation step and this effect has been assumed to negligibly impact the bending process.

Figures 3(a)–3(d) show SEM images of a bending NW at the extreme points of the deformation process. The NW shown in Fig. 3(b) was discretized along the length in order to measure the progressive bending as a function of the ion beam dose. A schematic of the bending of a single NW is shown in Fig. 3(e) with the x_s and z_s axes corresponding to the substrate normal and in-plane directions as viewed two dimensionally with the ion beam direction, B, always incident on the substrate at 45° with the origin located at the base of the wire. Thus, $B=\langle -1,-1\rangle$ in the vector notation. The shift of each section of the NW has been measured assuming a negligible variation along the perpendicular direction to the x_s-z_s plane. Thus, $z_s(x_s)$ is the displacement of the wire from the unbent state at position x_s. For the NW, it is useful to define x_w and z_w as the local Cartesian axes parallel and perpendicular to the irradiated side of the wire. Thus, in the unbent state, x_s and z_s are identical to x_w and z_w.

Since the ion beam and bent NW always remain in the x_s-z_s plane, a localized internal normal stress along x_w in the wire, $\sigma_{xx,w}$, is clearly being generated. In terms of explaining the origin of this stress, we first consider the ion hammering effect, which has been found to occur only in amorphous material systems including metallic, ceramic, and polymer glasses, thus suggesting that it is a universal ion irradiation response for the amorphous state.[21,22] No deformation occurs in materials that remain crystalline during ion bombardment. This ion-irradiation-induced deformation of amorphous solids has been explained in terms of a viscoelastic thermal spike model.[23] In this model, the deformation is attributed to the high degree of anisotropy of the ion-induced thermal spike. For high values of S_e, a cylindrical region around the ion track is heated. Assuming a positive thermal expansion coefficient, shear stresses generated by thermal expansion of the highly anisotropic heated region then relax, resulting in a local in-plane expansion perpendicular to the ion track that freezes in upon cooling of the thermal spike. The macroscopic anisotropic deformation is thus the result of a large number of individual ion impacts. High energy irradiation experiments indicated an apparent threshold of S_e $\sim$1 keV/nm below which no deformation would be expected[24] although Van Dillen *et al.*[25] demonstrated that ion irradiation at energies as low as 300 keV (S_e $\sim$0.4 keV/nm) can cause dramatic anisotropic plastic deformation in colloidal SiO_2 particles. According to ion hammering models,[26–30] in the case of a flat, planar sample with thickness greater than the projected ion range, R_p, being irradiated with the ion-beam incident at an angle of θ_i (relative to the surface normal), the generated in-plane stress along the direction coinciding with the surface projection of the ion beam will eventually reach a steady-state value of

$$\sigma_{xx,w} = -\tfrac{3}{2}A\,\eta\Phi\,\cos(2\theta_i), \tag{1}$$

where A is the deformation yield, η is the viscosity of the region experiencing viscous flow (the surface to the ion range), and Φ is the ion flux. The stress is considered steady state because the plastic flow behavior of the region is not changing with time, although plastic flow is occurring. This also corresponds to macroscopic deformation of the sample not changing with time. For the case of amorphous Ge under the presented irradiation conditions, $\eta\sim2\times10^{13}$ Pa s[31,32] and $\Phi=4.3\times10^{12}$ cm^{-2} s^{-1} with A further defined as[28]

$$A = 0.427\left(\frac{1+v}{5-4v}\right)\frac{\alpha S_e}{\rho c_p}, \tag{2}$$

where $v=0.28$ is the Poisson ratio,[3] $\alpha=7.9\times10^{-6}$ K^{-1} is the thermal expansion coefficient,[32] $S_e=0.12$ keV/nm assuming all energy lost is converted to heat,[32] $\rho=5.32$ g/cm^3 is the

Downloaded 17 Mar 2011 to 128.227.165.227. Redistribution subject to AIP license or copyright; see http://jap.aip.org/about/rights_and_permissions

density,[33] and $c_p = 0.4$ J/gK is the heat capacity of amorphous Ge.[34] Thus, assuming Eq. (2) can be extrapolated down to very low implant energies ($\ll \sim 0.5$ GeV) $A = 1.0 \times 10^{-2}$ nm^2 for Ga$^+$ implantation at 30 keV into amorphous Ge.

Thus, a significant discrepancy is now evident: the predicted steady-state values of $\sigma_{xx,w}$ are negative, since A is positive, and the side of the NW being irradiated is in a state of tension. Assuming that this model for the ion hammering holds, this would imply that the material has a negative value of the thermal expansion coefficient α, although α has been reported as positive for bulk Ge. Therefore, it can be concluded that the ion hammering model cannot explain the tensile stresses induced in the NWs unless a negative value of α is invoked. This would implicate that the mechanical properties of Ge would be markedly different at the nanoscale.

Rather than ion hammering, another possibility is that the irradiated side of the NW is experiencing densification, which has been reported to occur for other amorphous materials.[12] Irradiation-induced densification would result in a tensile stress on the irradiated side and cause a bending of the NW toward the ion beam, as is observed. The possible origin of densification is not known at present, although it is known that an amorphous structure can be perturbed from a "relaxed" state via irradiation, which may be partially responsible for such an effect.[35]

Using a basic beam bending argument analogous to Stoney's equation,[36] and assuming the ion-induced stress is occurring primarily within the projected range of the incident ions, the time-dependent nature of $\sigma_{xx,w}$, $\sigma(t)_{xx,w}$, generated in the NW can be calculated from the measured change in bending of the NW with irradiation dose using

$$\sigma_{xx,w}(t) = \frac{2EI[\theta_i(t)]}{\{w - R_p[\theta_i(t)]\}\Delta[\theta_i(t)]r(t)}, \quad (3)$$

where $E = 86$ GPa is the Young modulus of amorphous Ge,[32] I is the area moment of inertia of the section of NW beyond R_p as measured about the centroid of this section (assuming a circular cross-sectional area), w is the NW width, Δ is the cross-sectional area of the NW within R_p from the side being irradiated, and r is the radius of curvature of the NW. In each case, I, R_p, and Δ are dependent on θ_i which is itself time (t) dependent as evidenced by Fig. 3. The θ_i dependence of R_p is simply $R_p(\theta_i) = R_p(0)\cos(\theta_i)$, where $R_p(0) = 20$ nm is R_p at $\theta_i = 0°$ with the θ_i dependence of I and Δ attainable through basic integral calculus (not presented) and the t dependence of r measured using the sectioning process outlined previously. From Figs. 1 and 3(a)–3(d), the lower portion of the NWs is roughly straight such that θ_i can be reasonably assumed constant over this whole portion of the wire. The measured time (dose) dependence of $\sigma_{xx,w}$ [Eq. (3)] was compared with the steady-state value predicted to result from ion hammering [Eq. (1)] with θ_i at a given value of $t(Q)$, as shown in Fig. 3(f) with both values considered as averaged over the whole of the lower portion of the NWs. Only $t \geq 29$ s ($Q \geq 1.25 \times 10^{14}$ cm^{-2}) was considered in this analysis (approximately corresponding to the SEM images in Figs. 1(c)–1(e) since the NWs were fully amorphized for this regime. The error in $\sigma(t)_{xx,w}$ is reflective of the error in measuring $r(t)$ due to the possibility of minor misalignment during SEM imaging. Thus, a 10% error in $r(t)$ [corresponding to approximately the same relative error in $\sigma(t)_{xx,w}$] was adopted to sufficiently account for any minor imaging misalignments that may have arisen. It appears that the magnitudes of the measured stresses are very similar compared to the steady-state values predicted by ion hammering, although the sign of the stresses is opposite [Fig. 3(f)]. Therefore, a negative value of α of magnitude similar to that reported could be evoked to explain the results via ion hammering. Additionally, the time (dose) dependence of the magnitude of $\sigma_{xx,w}$ is similar to the magnitude of the steady-state stresses predicted by ion hammering as the measured stress in the NW increases as the wire continues to bend toward the beam (corresponding to increasing θ_i). Both of these characteristics imply that, assuming the ion hammering model is valid via a negative thermal expansion coefficient, the viscous flow behavior within the NWs is essentially always at equilibrium even though θ_i is changing with time. These results also suggest that the ion hammering effect is still possibly significant at low[24] electronic energy loss values ($S_e \sim 1$ keV/nm).

In terms of the densification argument, a simple volumetric strain argument suffices to estimate the amount of densification. The volumetric strain of the layer experiencing densification is given by $(\rho_f/\rho_0 - 1) = (\varepsilon_{xx} + \varepsilon_{yy} + \varepsilon_{zz})/3$, where ρ_f and ρ_0 are the densities of the material after and before irradiation and ε_{xx}, ε_{yy}, and ε_{zz} are the associated normal strains. In the case of uniaxial stress along $x(\sigma_{xx})$, $\varepsilon_{yy} = \varepsilon_{zz} = -\nu\varepsilon_{xx}$ and thus $\sigma_{xx} = 3E(\rho_f/\rho_0 - 1)/(1 - 2\nu)$. Using the previously mentioned material values, it is readily shown that a densification of $\sim 5\%$ (i.e., $\rho_f/\rho_0 \sim 1.05$) corresponds to σ_{xx} values on the order of several GPa which is similar to magnitudes calculated earlier. Thus, densification also provides a possible explanation for the observed ion-irradiation-induced NW bending. It is important to note that in bulk Ge, expansion, rather than densification, is observed. Thus, a discrepancy is also evident if the densification argument is to be used which implies the following: the response of the NWs to ion irradiation is fundamentally different from that occurs in bulk Ge material.

It is evident from Fig. 3 that mechanical work is being done on the NWs by the ion beam. The work done on the NW by the ion beam over of the time interval of implantation $t_1 \leq t \leq t_2$ is given by

$$W = \int_{t_1}^{t_2} \vec{F}_{\text{beam}}(t) \cdot \vec{v}_{\text{wire}}(t)dt, \quad (4)$$

where $\vec{F}_{\text{beam}}(t)$ is the t-dependent net force acting on the NW as generated by the ion beam and $\vec{v}_{\text{wire}}(t)$ is the t-dependent velocity of the NW measured at the NW center. The whole of the NW was considered for work analysis. The nature of $\vec{F}_{\text{beam}}(t)$ is dependent on the momentum of an incoming ion, $p_{\text{ion}} = 3.33 \times 10^{-20}$ N s, the time required for an ion to come to rest after impacting the surface, Δt_{rest}, and the number of ions instantaneously absorbed as a function of t, $N_{\text{inst}}(t)$. Thus, the force generated on the beam by the impact of a single ion is equal to $p_{\text{ion}}/\Delta t_{\text{rest}}$, with $N_{\text{inst}}(t)$ approximated as

Downloaded 17 Mar 2011 to 128.227.165.227. Redistribution subject to AIP license or copyright; see http://jap.aip.org/about/rights_and_permissions

$$N_{\text{inst}}(t) \sim \Delta t_{\text{rest}} \frac{\Phi}{\sqrt{2}} w \int_0^{h_p(t)} \left(\frac{\partial z_s(t)}{\partial x_s} - 1 \right) dx_s, \tag{5}$$

where $h_p(t)$ is the projected height of the NW as a function of t and $w \sim 50$ nm is the cross-sectional width of the wire. Thus, $\vec{F}_{\text{beam}}(t)$ in vector notation is approximated as

$$\vec{F}_{\text{beam}}(t) \sim p_{\text{ion}} \frac{\Phi}{2} w \int_0^{h_p(t)} \left(\frac{\partial z_s(t)}{\partial x_s} - 1 \right) dx_s \langle -1, -1 \rangle, \tag{6}$$

with typical values of $\vec{F}_{\text{beam}}(t)$ on the order of $\sim 0.1 \times 10^{-15}$ N.

Numerically computing the integral in Eq. (4) for $29 \leq t \leq 143$ s (corresponding to $1.25 \times 10^{14} \leq Q \leq 6.15 \times 10^{14}$ cm^{-2} where the NWs have been fully amorphized) produces $W = \sim -3 \pm 1$ eV. It should be noted that these values are orders of magnitude lower than the work required to elastically bend nonirradiated crystalline Si NWs over comparable length scales.[37] Therefore, our experiment clearly shows that it is easier to perform mechanical work during ion irradiation of an amorphous material compared to the crystalline counterpart.

The ion beam can shape the NW as desired, and thus loops or springs can be realized by suitably changing the impinging beam location and direction. Therefore, using a similar procedure, it is presumably possible to bend Si or SiO_2 NWs, although it may be the case that compressive, rather than tensile stresses, would be generated in the irradiated side of the NW, depending on how the beam interacts with a specific material.[38] In the case of SiO_2, the capability of directly modifying the NW shape may open up additional opportunities for making versatile building blocks for micro- and nanoscale photonic circuits and components,[39] as well as functionalizing photonic glasses on the nanometer scale.

IV. CONCLUSIONS

In conclusion, ion beam-induced deformation of Ge NWs was presented. Large reversible bending of the wires toward the incident beam direction is observed. This bending is indicative of the irradiated side of the structure experiencing tensile stress and could not be attributed to the ion hammering effect without the use of a negative thermal expansion coefficient. Another possible explanation is that the material is experiencing densification during irradiation. Although the mechanism is not yet understood in detail, the deformation of the structures is highly reproducible and suitable for *in situ* manipulation of three-dimensional shapes by FIBs.

ACKNOWLEDGMENTS

The authors acknowledge the Major Analytical Instrumentation Center at the University of Florida for use of the transmission electron microscope and FIB facilities, and Clarence Tracy at Arizona Institute of Nanoelectronics (Arizona State University, Tempe) for his work and guidance on patterning substrates. This work was performed, in part, at the Center for Integrated Nanotechnologies, a U.S. Department of Energy, Office of Basic Energy Sciences user facility, Los Alamos National Laboratory (Contract No. DE-AC52-06NA25396) site.

[1] R. S. Wagner and W. C. Ellis, Appl. Phys. Lett. **4**, 89 (1964).
[2] Y. Cui and C. M. Lieber, Science **291**, 851 (2001).
[3] P. Agarwal, M. N. Vijayaraghava, F. Neuilly, E. Hijzen, and G. A. M. Hurkx, Nano Lett. **7**, 896 (2007).
[4] B. Tian, X. Zheng, T. J. Kempa, Y. Fang, N. Yu, G. Yu, J. Huang, and C. M. Lieber, Nature (London) **449**, 885 (2007).
[5] S. M. Koo, A. Fujiwara, J. P. Han, E. M. Vogel, C. A. Richter, and J. E. Bonevich, Nano Lett. **4**, 2197 (2004).
[6] J. Martinez, R. V. Martínez, and R. Garcia, Nano Lett. **8**, 3636 (2008).
[7] A. Tribu, G. Sallen, T. Aichele, R. André, J. P. Poizat, C. Bougerol, S. Tatarenko, and K. Kheng, Nano Lett. **8**, 4326 (2008).
[8] L. S. Robertson, K. S. Jones, L. M. Rubin, and J. Jackson, J. Appl. Phys. **87**, 2910 (2000).
[9] A. V. Krasheninnikov and F. Banhart, Nature Mater. **6**, 723 (2007).
[10] M. A. Nastasi, J. W. Mayer, and J. K. Hirvonen, *Ion-Solid Interactions: Fundamentals and Applications* (Cambridge University Press, Cambridge, England, 1996).
[11] S. Klaumünzer and G. Schumacher, Phys. Rev. Lett. **51**, 1987 (1983).
[12] E. Snoeks, A. Polman, and C. A. Volkert, Appl. Phys. Lett. **65**, 2487 (1994).
[13] L. Tong, R. R. Gattass, J. B. Ashcom, S. He, J. Lou, M. Shen, I. Maxwell, and E. Mazur, Nature (London) **426**, 816 (2003).
[14] B. Stritzker, R. G. Elliman, and J. Zou, Nucl. Instrum. Methods Phys. Res. B **175–177**, 193 (2001).
[15] B. C. Park, K. Y. Jung, W. Y. Song, O. Beom-hoan, and S. J. Ahn, Adv. Mater. (Weinheim, Ger.) **18**, 95 (2006).
[16] S. K. Tripathi, N. Shukla, S. Dhamodaran, and V. N. Kulkarni, Nanotechnology **19**, 205302 (2008).
[17] W. J. Arora, S. Sijbrandij, L. Stern, J. Notte, H. L. Smith, and G. Barbastathis, J. Vac. Sci. Technol. B **25**, 2184 (2007).
[18] S. I. Novikova, *Thermal Expansion of Crystals* (Science, Moscow, 1974).
[19] J. F. Ziegler, J. P. Biersack, and U. Littmark, *The Stopping and Range of Ions in Solids* (Pergamon, New York, 2003).
[20] D. Hickey, Ph.D. thesis, University of Florida, 2007.
[21] A. Hedler, S. L. Klaumünzer, and W. Wesch, Nature Mater. **3**, 804 (2004).
[22] A. Benyagoub, S. Loffler, M. Rammensee, S. Klaumünzer, and G. Saemann-Ischenko, Nucl. Instrum. Methods Phys. Res. B **65**, 228 (1992).
[23] H. Trinkaus and A. I. Ryazanov, Phys. Rev. Lett. **74**, 5072 (1995).
[24] E. Snoeks, A. van Blaaderen, T. van Dillen, C. M. van Kats, M. L. Brongersma, and A. Polman, Adv. Mater. (Weinheim, Ger.) **12**, 1511 (2000).
[25] T. van Dillen, A. Polman, C. M. van Kats, and A. van Blaaderen, Appl. Phys. Lett. **83**, 4315 (2003).
[26] S. Klaumünzer, C. Li, S. Löffler, M. Rammensee, G. Schumacher, and H. C. Neitzert, Radiat. Eff. Defects Solids **108**, 131 (1989).
[27] A. Benyagoub, S. Löffler, M. Rammensee, and S. Klaumünzer, Radiat. Eff. Defects Solids **110**, 217 (1989).
[28] S. Klaumünzer and A. Benyagoub, Phys. Rev. B **43**, 7502 (1991).
[29] A. Gutzmann, S. Klaumünzer, and P. Meier, Phys. Rev. Lett. **74**, 2256 (1995).
[30] A. Gutzmann and S. Klaumünzer, Nucl. Instrum. Methods Phys. Res. B **127–128**, 12 (1997).
[31] C. A. Volkert, J. Appl. Phys. **70**, 3521 (1991).
[32] A. Witvrouw and F. Spaepen, J. Appl. Phys. **74**, 7154 (1993).
[33] C. Mathioudakis and P. C. Kelires, J. Non-Cryst. Solids **266–269**, 161 (2000).
[34] W. Szyszko, F. Vega, and C. N. Afonso, Appl. Phys. A: Mater. Sci. Process. **61**, 141 (1995).
[35] S. Roorda, W. C. Sinke, J. M. Poate, D. C. Jacobson, S. Dierker, B. S. Dennis, D. J. Eaglesham, F. Spaepen, and P. Fuoss, Phys. Rev. B **44**, 3702 (1991).
[36] G. Stoney, Proc. R. Soc. London, Ser. A **82**, 172 (1909).
[37] S. Hoffmann, I. Utke, B. Moser, S. H. Christiansen, V. Schmidt, U. Golsele, and C. Ballif, Nano Lett. **6**, 622 (2006).
[38] J. Nord, K. Nordlund, and J. Keinonen, Phys. Rev. B **65**, 165329 (2002).
[39] J. W. Dailey, J. Taraci, T. Clement, D. J. Smith, J. Drucker, and S. T. Picraux, J. Appl. Phys. **96**, 7556 (2004).

Downloaded 17 Mar 2011 to 128.227.165.227. Redistribution subject to AIP license or copyright; see http://jap.aip.org/about/rights_and_permissions